Prior image based temporally constrained reconstruction algorithm for magnetic resonance guided high intensity focused ultrasound

Jaya Prakash[a)]
Institute of Biological and Medical Imaging, Helmholtz Zentrum Munich, Ingolstaedter Landstraße 1, Munich D-85764, Germany and Supercomputer Education and Research Centre, Indian Institute of Science, Bangalore 560012, India

Nick Todd
Wellcome Trust Centre for Neuroimaging, UCL Institute of Neurology, University College London, London WC1N 3BG, United Kingdom

Phaneendra K. Yalavarthy
Supercomputer Education and Research Centre, Indian Institute of Science, Bangalore 560012, India

(Received 18 December 2014; revised 15 October 2015; accepted for publication 18 October 2015; published 6 November 2015)

Purpose: A prior image based temporally constrained reconstruction (PITCR) algorithm was developed for obtaining accurate temperature maps having better volume coverage, and spatial, and temporal resolution than other algorithms for highly undersampled data in magnetic resonance (MR) thermometry.
Methods: The proposed PITCR approach is an algorithm that gives weight to the prior image and performs accurate reconstruction in a dynamic imaging environment. The PITCR method is compared with the temporally constrained reconstruction (TCR) algorithm using pork muscle data.
Results: The PITCR method provides superior performance compared to the TCR approach with highly undersampled data. The proposed approach is computationally expensive compared to the TCR approach, but this could be overcome by the advantage of reconstructing with fewer measurements. In the case of reconstruction of temperature maps from 16% of fully sampled data, the PITCR approach was 1.57× slower compared to the TCR approach, while the root mean square error using PITCR is 0.784 compared to 2.815 with the TCR scheme.
Conclusions: The PITCR approach is able to perform more accurate reconstructions of temperature maps compared to the TCR approach with highly undersampled data in MR guided high intensity focused ultrasound. © *2015 American Association of Physicists in Medicine.* [http://dx.doi.org/10.1118/1.4934829]

Key words: MR thermometry, dynamic imaging, MRgHIFU, image reconstruction, temperature maps

1. INTRODUCTION

Noninvasive local heating of tissues deep inside the human body can be accomplished using high-intensity focused ultrasound (HIFU).[1,2] Magnetic resonance imaging (MRI) provides images which enable excellent visualization of anatomical structures and tumors, resulting in better treatment planning.[3] MRI can also provide continuous temperature maps based on the proton resonance frequency (PRF) shift of water with good spatial and temporal resolution for real-time magnetic resonance (MR) thermometry.[4,5] Thermal therapies through the human skull using MR guided high intensity focused ultrasound (MRgHIFU) require effective monitoring of 3D temperature maps. These applications require MRgHIFU to perform imaging over larger volumes, provide high spatiotemporal resolution for accurate tracking of rapid heating at the focal point, and monitoring the heating in the near- and far-fields of the ultrasound beam.[6,7] The methods for accurate reconstruction of large-field of view (FOV) undersampled temperature data sets in MRgHIFU applications[8] include model predictive filtering (MPF),[9] temporally constrained reconstruction (TCR),[10] and parallel imaging with unaliasing by Fourier encoding of the overlaps using the temporal dimension (UNFOLD).[11]

Model predictive filtering requires prior knowledge of the tissue acoustic and thermal properties for accurate estimation of temperature maps.[9] This method uses the Pennes bioheat equation as a model, along with tissue acoustic properties, to obtain the temperature distribution. A potential limiting factor of this method is the requirement to accurately estimate many tissue dependent parameters,[9] and therefore MPF was not utilized for comparison with the proposed scheme. Parallel imaging with UNFOLD method is not capable of monitoring the entire 3D volume of interest, as this scheme uses a spatially selective RF pulse (2DRF) which assumes that only a small part of the FOV is imaged.[11] Parallel imaging results in aliasing artifacts, which can be later removed using the UNFOLD scheme.[11] The TCR approach is a method that has the ability to provide large coverage 3D temperature maps.[12] Therefore, this approach was used to validate the proposed algorithm.

The critical aspect of MRgHIFU temperature map estimation lies with obtaining the temperature maps in real-time.[13] Moreover, the ability to estimate the temperature maps with less data is also highly desirable in many clinical scenarios, as it also reduces the scan time. Hence, obtaining accurate temperature maps with fewer measurements and estimating the temperature maps in real-time plays a vital role in MRgHIFU. It is important to note that the ultrasound is focused on a specific region of interest (ROI) (highly localized), leading to an increase in temperature at the region of interest [making the temporal changes in temperature (phase) sparse]. Therefore, reconstruction of the MR 3D temperature maps becomes a sparse recovery problem. Previously, the TCR approach was used to accurately estimate the temperature maps by imposing a smoothness/sparsity constraint using a temporal gradient.[10,12,14] Note that the temporally constrained reconstruction is one of the well-established approaches to estimate the temperature maps in MRgHIFU;[14] thus, the proposed scheme is compared with TCR as the benchmark.

The TCR based algorithm enables a data compression of the order of 2–6× (17%–50% data), but this approach does not provide the high level of data optimization that is required, especially when the desirable compressed data is around 12× (8%). A prior image constrained compressive sensing (PICCS) algorithm has been proposed in dynamic computed tomography (CT), wherein it has been shown that incorporating a prior image as a constraint can result in better reconstruction with relatively few projections.[15,16] Note that in CT, high undersampling will help reduce dosage, while in MRI, it helps reduce scan times (desirable in real-time MRI imaging). Hence in this work, an additional constraint based on the prior image (either the previous or next time frame) is applied and shown to provide increased accuracy at very high undersampling rates.

Recent studies in MR thermometry have shown that the usage of a ℓ_0-norm penalty on the phase shift of the temperature can result in an estimation of the temperature maps with fewer measurements.[17,18] This constraint was implemented using an iteratively reweighted least squares approach. Other studies have proposed fitting the model directly to the baseline images along with an ℓ_1-norm based minimization.[19] Complex difference compressive sensing has also been proposed, where baseline images were obtained before heating and included as a constraint.[20] In this paper, a variation of PICCS, to be called prior image based temporally constrained reconstruction (PITCR), is presented and shown to produce accurate temperature maps with fewer MR measurements. The PITCR method performs the temperature map estimation by applying a smoothness constraint and also giving weight to the prior image, resulting in an improved temperature map estimation. In contrast, existing complex difference compressive sensing employs the baseline images acquired before heating, while in the proposed scheme, the prior image is generated using the previous gradient iteration update. The proposed PITCR algorithm is implemented to provide high spatial and temporal resolution covering a large 3D volume. The proposed scheme is found to be more robust to data noise. The performance of the PITCR is also evaluated in the presence of motion outside the FOV.

2. METHODS

2.A. TCR

A discrete inverse Fourier transform based reconstruction (considered as truth for comparison with TCR and PITCR) from the full k-space data can be written as[10]

$$d = Fm, \tag{1}$$

where the 4D full k-space data acquired at various time frames is represented by d and the complex MR image is represented by m (having dimension $M\times N\times L\times T$, where $M\times N\times L$ represents the spatial dimensions corresponding to the x, y, and z axis, respectively, and T represents the temporal dimension). Here, F indicates the 2D Fourier transform at each time frame in a dynamic sequence along the y-dimension.

The temperature distribution is obtained using a TCR algorithm, where a data fidelity term is applied while constraining the rapid temporal change. The undersampled sparse data ($\tilde{d}$) are acquired (and the unacquired data points are 0), for which the reconstruction is performed by minimizing the cost function represented as[10,12,14]

$$\min_{\tilde{m}}\{\lambda \parallel (\Delta\tilde{m}) \parallel_2^2 + \parallel WF\tilde{m} - \tilde{d} \parallel_2^2\}, \tag{2}$$

where the 4D binary sparsifying pattern is represented by W (of dimension $N\times N$, representing here sample phase encoded lines) to obtain $\tilde{d}$ (of dimension $M\times N\times L\times T$) from d (of dimension $M\times N\times L\times T$). The λ is a scalar which acts like a regularization parameter, and Δ represents the temporal derivative. This objective function can now be minimized using a gradient descent approach with finite forward difference method, leading to a series of image frames updated iteratively as[10]

$$\tilde{m}^{n+1} = \tilde{m}^n - \epsilon_s C'(\tilde{m}^n); \quad n = 0,1,2,\ldots,100, \tag{3}$$

where ϵ_s represents the step size corresponding to the gradient descent approach and $C'(\tilde{m})$ represents the Euler–Lagrange derivative of the objective function given as[10]

$$C'(\tilde{m}) = 2*(F^{-1}(WF\tilde{m}) - F^{-1}(\tilde{d}) - \lambda\Delta_t^2\tilde{m}), \tag{4}$$

where Δ_t^2 denotes the temporal Laplacian and operates on the complex data. The TCR algorithm takes advantage of the Laplacian across frames (previous time point) to reconstruct the temperature maps.

The TCR algorithm is applied in an ℓ_1-norm based framework, where the following cost function is minimized:[10,12,14]

$$\min_{\tilde{m}}\{\lambda_{l1} \parallel (\Delta\tilde{m}) \parallel_1 + \parallel WF\tilde{m} - \tilde{d} \parallel_2^2\}, \tag{5}$$

where λ_{l1} is the regularization parameter. The ℓ_1-norm is approximated using the following relation $\|\Delta\tilde{m}\|_1 = \sqrt{(\Delta\tilde{m})^2 + \beta}$ with $\beta = 10^{-6}$ in this work.[21] The Euler–Lagrange derivative of the above function,

$$C'(\tilde{m}) = 2*\left(F^{-1}(WF\tilde{m}) - F^{-1}(\tilde{d}) - \lambda_{l1}\frac{\Delta\tilde{m}}{\sqrt{\beta + (\Delta\tilde{m})^2}}\right), \tag{6}$$

is used in the finite forward difference scheme. The regularization parameter (λ and λ_{l1}) is optimally chosen using a L-curve[22] or L1-curve[23] based methods.

2.B. PITCR

While TCR applies a temporal constraint to perform the image reconstruction, the PITCR algorithm has an additional constraint to include the temporal constraint that utilizes either the previous or the next time frame. The usage of undersampled data for reconstruction induces aliasing artifacts, which are removed by usage of penalty terms (that act like filters) in the TCR algorithm. The usage of a prior image in the dynamic sequence along with the regularization penalty allows for better image reconstruction with fewer measurements in the PITCR algorithm. This approach minimizes the unconstrained variant, namely,

$$\min_{\tilde{m}}\{\tilde{\lambda}[\alpha \parallel \triangle(\tilde{m}-\tilde{m}_{pr}) \parallel_2^2 + (1-\alpha) \parallel (\triangle\tilde{m}) \parallel_2^2] + \parallel F\tilde{m}-\tilde{d} \parallel_2^2\}, \quad (7)$$

with $\tilde{\lambda}$ representing the non-negative regularization parameter and $\tilde{m}_{pr}$ being the prior information calculated from the previous or the next time frame. The prior image for the proposed scheme is defined as

$$\tilde{m}_{pr} = \begin{cases} \tilde{m}_{j+1} & \text{if } j > t*, \\ \tilde{m}_{j-1} & \text{if } j < t*, \end{cases} \quad (8)$$

where t^* represents the frame at which the temperature reaches a maximum. In practice, one can record when the ultrasound is turned on and off for HIFU heating, and the occurrence of the maximum temperature coincides with the time point at which the ultrasound is turned off. In this work, turning on and off of the ultrasound is not measured and it is difficult to estimate the maximum temperature peak before performing the reconstructions. Therefore, it was assumed that the maximum peaks occurs at $t^* = T/2$ (where T indicates the total number of time frames). The reason for selecting this prior image is that if the maximum temperature is increasing, the previous time frame should act as the prior image and when the maximum temperature decreases the next time frame should act as the prior image. This prior image was computed based on the previous gradient descent iteration update ($\tilde{m}^n$ at iteration $n+1$). For example, at gradient descent iteration 10, the prior term is computed based on the solution obtained at the gradient descent iteration 9. Note that the first time point reconstruction is performed with fully sampled k-space data, and the next time points have undersampled k-space data (similar to the TCR algorithm). To evaluate the performance of the proposed PITCR method [defining prior term as in Eq. (8)] with the first frame based image reconstruction, the prior image is considered to be the first frame, i.e., $\tilde{m}_{pr} = \tilde{m}_0$ with $\tilde{m}_0$ indicating the first frame reconstructed with all the data. The weight factor is represented by α ($\alpha = 0$ indicates reconstruction using the TCR approach and $\alpha = 1$ indicates full weight given for the prior image). Note the above weights were used as α and $1-\alpha$ based on Ref. 15, but one can choose the weights as α and β to improve the reconstruction accuracy, at the cost of increasing the number of reconstruction parameters. Equation (7) can be solved employing a gradient descent approach with finite forward difference method using Eq. (3). The Euler–Lagrange derivative $[C(\tilde{m})]$ of the PITCR objective function becomes

$$C(\tilde{m}) = 2*(F^{-1}(WF\tilde{m}) - F^{-1}(\tilde{d}) - \lambda((1-\alpha)*\Delta_t^2\tilde{m}) - \lambda(\alpha*\Delta_t^2(\tilde{m}-\tilde{m}_{pr}))). \quad (9)$$

The steps of the PITCR algorithm for the 4D temperature map reconstruction are shown in Algorithm I. The forward difference step and Euler–Lagrange derivative estimation should be performed using the above equation. Note that in both the TCR and PITCR algorithms, the sliding window reconstruction is used as the initial image estimate (current TCR works in this fashion). A note about the convergence of the PITCR approach can be found in the Appendix. The comparison of the proposed scheme is done using *ex vivo* pork muscle experiments, which will be discussed in Sec. 2.C.

2.C. Simulation and experiments

The PITCR method was evaluated using experimentally measured MRgHIFU data sets. The HIFU heating was performed in a Siemens TIM Trio MRI scanner (Siemens Medical Solutions, Erlangen, Germany) using an MRI-compatible phased array transducer (256 elements, 13 cm radius of curvature, 1 MHz frequency, Imasonic, Besancon, France and Image Guided Therapy, Pessac, France). A 3D segmented EPI gradient echo sequence was used for imaging in all experiments conducted here.[13]

In the first set of experiments, HIFU heating experiments were performed on an *ex vivo* pork muscle sample at 36 acoustic watts for 30 s; the rate of change in temperature at this power level was 2.2 °C/s.[13] Under identical circumstances, the heating was repeated twice at this power level. During the first heating, the imaging parameters were chosen such that the 3D volume could be fully sampled at sufficient temporal resolution. These fully sampled data sets were reconstructed by means of the standard Fourier transform approach and used to compute temperature maps (this was considered as truth). Imaging parameters for the fully sampled data were $128\times72\times12$ imaging matrix (10 slices plus 20% slice oversampling), $1.5\times1.5\times3.0$ mm resolution, TR = 25 ms, TE = 10 ms, EPI factor = 9, bandwidth = 738 Hz/pixel, flip angle = 20°, and time interval of 2.4 s/scan. Then the proposed PITCR and TCR reconstruction methods utilized the undersampled version of the acquired data, and the reconstructions were performed by sampling 33% and 16% of the acquired fully sampled data.

The TCR and PITCR temperature map estimation was carried out for larger 3D volumes that were acquired at an undersampling factor of 6. Each pair of identical heating runs was performed at the same location in the sample. Imaging parameters for the undersampled data were $1.5\times1.5\times3.0$ mm resolution, $128\times108\times24$ imaging matrix (22 slices plus 9% slice oversampling), TR = 25 ms, TE = 10 ms, EPI factor = 9, bandwidth = 738 Hz/pixel, flip angle = 20°, 6× undersampling, and time interval of 1.2 s per undersampled time frame.[13] This undersampled data were used to obtain the temperature maps with the TCR and the proposed PITCR algorithms, and then compared with the standard Fourier transform

ALGORITHM I. PITCR.

INPUT: $\tilde{d}$ (4-D Undersampled k-space data), W (4-D Sampling Pattern),
$\tilde{\lambda}$ (Regularization Parameter), α (Weight Parameter), N_{it} (Number of iterations), st (time frames)
OUTPUT: m (4-D Output Temperature map)

1. Compute the Sliding Window k-space and initial image estimate; $d_{SW} = F(SW(\tilde{d}.*W))$, $m_{SW} = F'(d_{SW})$;
2. Initialize necessary variable; Sparse Image Estimate ($m_{est} = F'(\tilde{d}.*W)$), Image Estimate using SW using Fourier operator along 1st and 3rd dimension ($m = F(F(m_{SW},1),3)$)

for i=1 to N_{it}

3. k-space ($\check{d}$) estimate from Image Estimate; $\check{d} = F(m,2)$
4. Sparse k-space ($\tilde{d}$) obtained from Sampling Pattern; $\hat{d} = \check{d}.*W$.
5. Sparse Image Estimate from ($\hat{d}$); $\tilde{m} = F'(\hat{d},2)$
6. Gradient of Fidelity Term; $\delta = m_{est} - \tilde{m}$
7. Forward Difference of the Image Estimate; $\triangle m_{fwd}(:,:,:,1:st-1) = m(:,:,:,2:st)$; $\triangle m_{fwd}(:,:,:,st) = m(:,:,:,st)$
8. Backward Difference of the Image Estimate; $\triangle m_{back}(:,:,:,2:st) = m(:,:,:,1:st-1)$; $\triangle m_{back}(:,:,:,1) = m(:,:,:,1)$
9. Temporal Laplacian Estimate; $\Delta^2 m_t = \triangle m_{fwd} - 2*m + \triangle m_{back}$

for $t = 1$ to st
if $t < \frac{st}{2}$
if $t == 1$
10. $m_{pr}(:,:,:,1) = m(:,:,:,1)$
else
11. $m_{pr}(:,:,:,t) = m(:,:,:,t-1)$
end
else
if $t == st$
12. $m_{pr}(:,:,:,t) = m(:,:,:,t)$
else
13. $m_{pr}(:,:,:,t) = m(:,:,:,t+1)$
end
end
end
14. $\triangle_t m_{pr} = m - m_{pr}$; $\Delta = \delta + (1-\alpha)*\tilde{\lambda}*\Delta^2 m_t + \alpha*\tilde{\lambda}*\triangle_t^2 m_{pr}$; $m = m + \Delta$
end
15. $m = F'(F'(m,1),3)$

reconstruction performed with full data. The obtained 6× undersampled dataset was further undersampled by 50% and the reconstruction was performed using this highly undersampled data to bring out the potential of the proposed method. The same data were used to compare the proposed scheme by applying a constraint employing the first frame.

The PITCR method was also evaluated with noisy 6× data. Zero-mean Gaussian random noise was added to the undersampled k-space data, such that the sliding window reconstruction of the noisy k-space produced temperature maps with temperature standard deviations of 1.02 °C as measured over the ROI. These noisy data were used to perform the reconstruction using the TCR and the proposed PITCR approach. The obtained noisy data were further undersampled by 50% and the reconstruction was performed to determine the performance of the PITCR scheme compared to TCR method in highly undersampled data cases.

To verify the performance of the proposed method using a motion data case, a HIFU heating of a pork muscle sample was performed. Periodic motion was generated by placing above the sample a water-filled balloon which was periodically compressed. The pork sample was not moved, but the balloons changing volume affected the phased data obtained, resulting in disturbances to the temperature maps. The imaging parameters were similar to those described above with 3D data acquisition and 6× undersampling. The balloon compression was designed to mimic phase disturbances due to chest motion from the breathing cycle and was compressed at a rate of roughly once every 25 s. The data were undersampled as described in Ref. 12. In brief, the data were fully sampled along the partition direction (k_z or "slow" phase encoding direction) and undersampled along the phase encoding direction (k_y). The 3D data were acquired using a multishot EPI approach, where the EPI factor denotes the number of echoes acquired in each echo train. These echoes are evenly spaced in k_y. An in-house built 4-channel surface coil was utilized for the data acquisition. The algorithms do not make use of coil sensitivity profiles, either measured or estimated. For a detailed analysis of various sampling strategies, see Ref. 24. The image reconstruction was carried out on a machine with an Intel Xeon dual six core processor with a processor speed of 2.66 GHz and memory of 64 GB.

3. RESULTS

The fully sampled data obtained from the MRI scanner were undersampled to have only 33% and 16% of the acquired

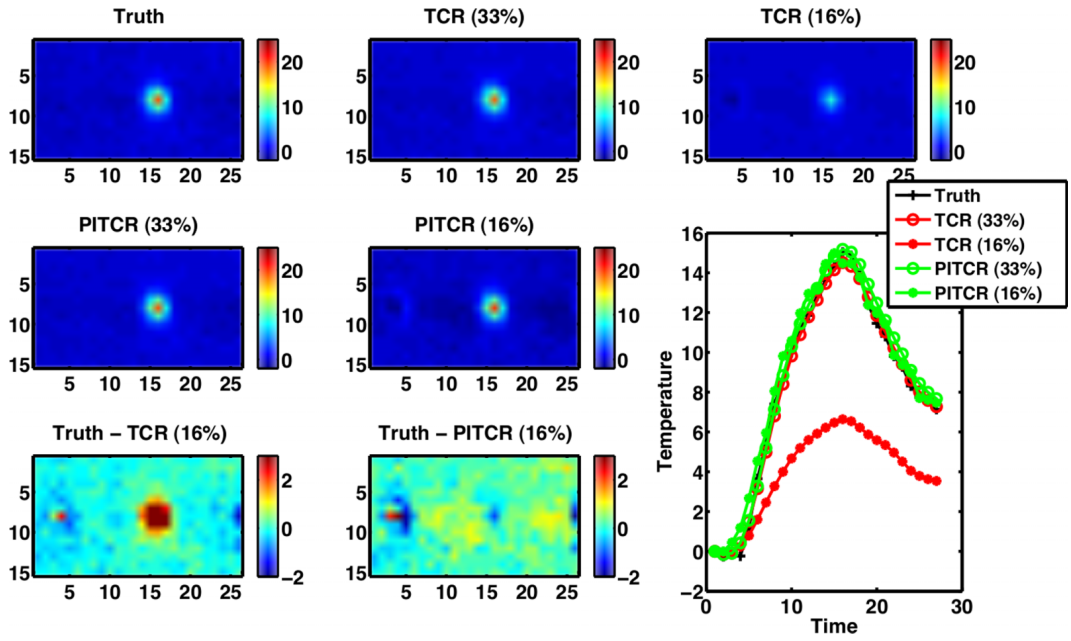

FIG. 1. Comparison of temperature map reconstruction of the standard TCR with PITCR method. The reconstruction was performed using 33% and 16% of the acquired fully sampled data. Difference image is also shown for better comparison of reconstructed temperature distribution. The plots show the maximum temperature increase over time in the HIFU heating.

data, which was then used for estimating the temperature maps using the TCR and the PITCR method. Figure 1 shows the temperature map reconstruction, the difference between the reconstructed temperature maps and the truth (reconstructed with Fourier transform approach having full data), and the maximum temperature over time graph. When less data are available, the PITCR method provides a significantly better estimation of the temperature than the TCR algorithm. The weight parameter α was kept as 0.3 for all cases in this work. The computational time along with the root mean square error (RMSE) is reported in Table I. The RMSE was calculated over a $5\times5\times7$ voxel region at the region of interest over all the time points as used in Ref. 12. The number of gradient descent iterations was 100 in all cases. The reconstruction parameter λ was selected optimally using an L-curve method, and for this particular case, the λ was found to be 0.0491 and 0.0451 for 33% and 16% data cases, respectively. The regularization parameter ($\tilde{\lambda}$) for the PITCR method was set at 0.05 in both cases [note that ($\tilde{\lambda}$) was chosen heuristically in this work due to the huge computational cost associated with estimating $\tilde{\lambda}$ using the L-curve method].

The reconstructed temperature distribution using the 6× undersampled data obtained from the MRI scanner for the standard TCR and the proposed PITCR method is shown in Fig. 2. These data were further undersampled by 50%, and the reconstruction results pertaining to these data were also shown in Fig. 2. The 1D plot (temperature over time) in Fig. 2 shows that both TCR and PITCR results in similar reconstructions when the full 6× undersampled data were utilized, while PITCR outperforms TCR when fewer measurements are available. Hence, it can be concluded that the PITCR algorithm works better than TCR algorithm with highly undersampled data, as can be observed from the RMSE values in Table I. Note that the reconstruction pertaining to the ℓ_1-norm based TCR is also compared with PITCR in Fig. 2. The proposed scheme is able to estimate the temperature distribution better than the ℓ_1-norm based TCR approach. The regularization parameter (λ) for the TCR algorithm is optimally selected using the L-curve and L1-curve method as shown in Fig. 3. The reconstruction parameter (λ) used for the TCR algorithm (using ℓ_2-norm) was 0.0931 and 0.0951 for 17% and 8.5% data cases, while in the ℓ_1-norm case, the parameters were found to be

TABLE I. Comparison of computational time and RMSE for the results presented in this work. The percentage of *k*-space data used is given in the parenthesis. The results show that the PITCR method has superior performance compared to TCR with fewer measurements.

	Fully sampled data (Fig. 1)				Undersampled data (Fig. 2)			
Method	PITCR (33%)	PITCR (16%)	TCR (33%)	TCR (16%)	PITCR (17%)	PITCR (8.5%)	TCR (17%)	TCR (8.5%)
Data acquisition time	1	0.5	1	0.5	1	0.5	1	0.5
Reconstruction time (time in seconds)	1.66 (11.104)	1.57 (11.65)	1 (6.67)	1 (7.39)	1.61 (89.86)	1.63 (88.48)	1 (55.62)	1 (54.32)
Total time	2.66	2.07	2	1.5	2.61	2.13	2	1.5
RMSE (in °C)	0.242	0.784	0.235	2.815	0.43	0.56	0.42	1.24

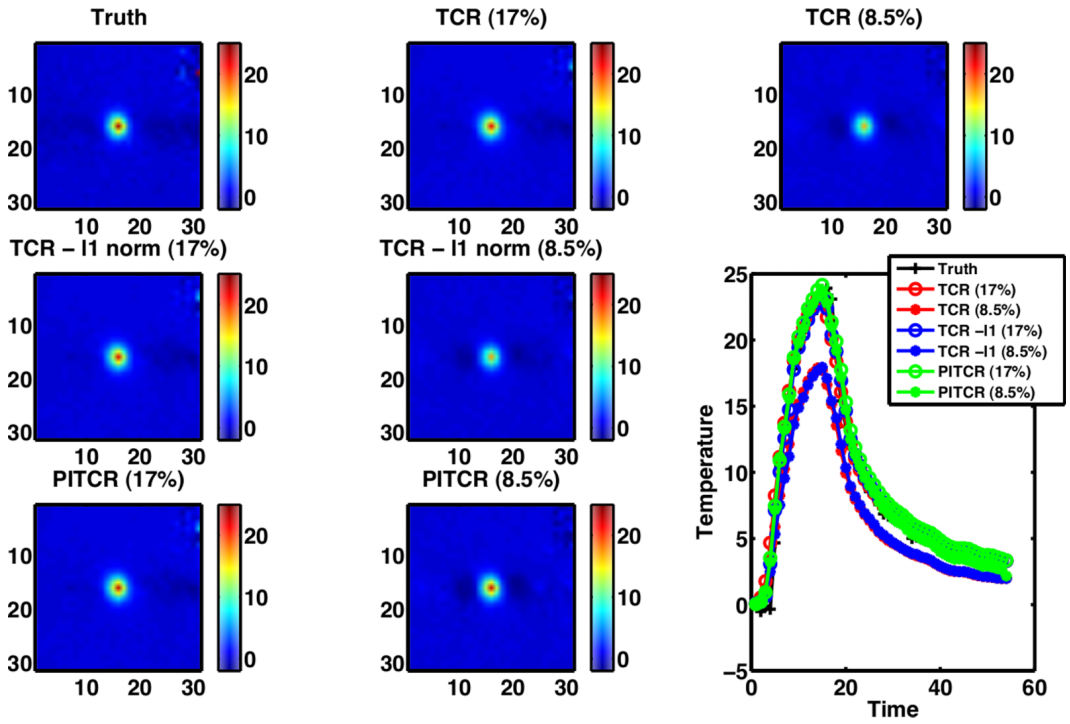

FIG. 2. Comparison of temperature map reconstruction of the standard TCR with PITCR method. The sampling used is shown in the parenthesis. The plots show the maximum temperature increase over time with 6× undersampling and for acquired 6× undersampled data further reduced by 50%.

0.12 and 0.15 for 17% and 8.5% data cases. The regularization parameter used for PITCR method was 0.005 in these cases.

To show the effectiveness of the PITCR method in a noisy environment with few measurements, noise that mimics the coil induced errors was added to the obtained undersampled MRI data (6× undersampling). The resultant noisy data were undersampled by 50%, and then temperature maps were reconstructed from this highly undersampled data using the TCR and the PITCR methods. The reconstruction distribution using 17% and 8.5% measurements is shown in Fig. 4, along with the maximum temperature versus time plot for all reconstructions. The reconstruction indicates that the proposed scheme is robust in noisy environments and is able to reconstruct the temperature distribution more accurately than the TCR algorithm with fewer measurements, leading to faster data collection. The reconstruction parameter (λ) for the TCR algorithm

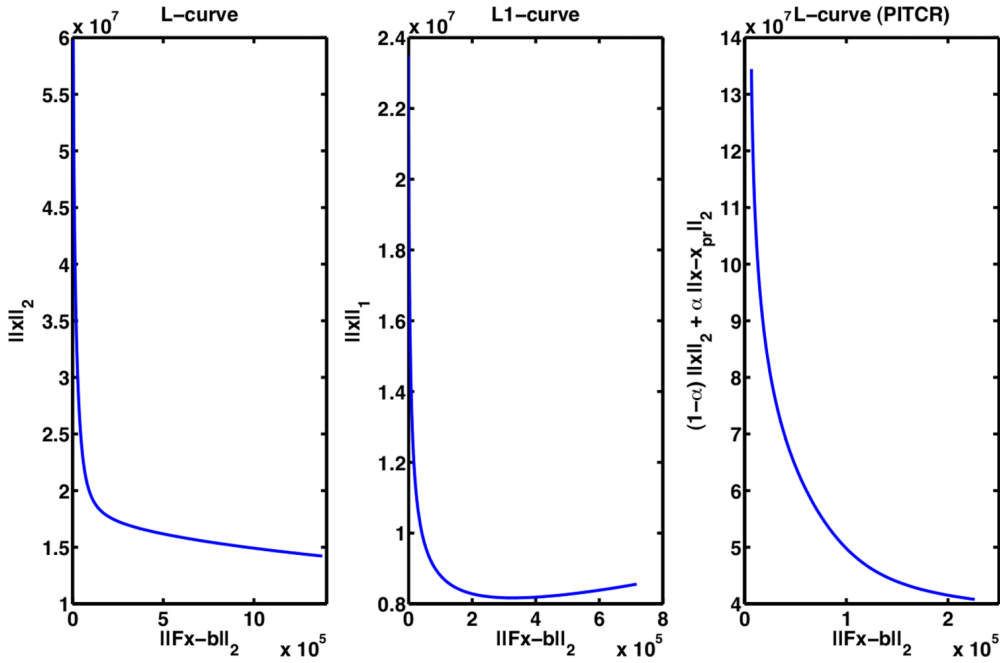

FIG. 3. L-curve and L1-curve based method used for estimating optimal regularization parameter. The optimal regularization was found to be 0.0931 and 0.12 for the TCR with ℓ_2 and ℓ_1-norm based reconstruction. The optimal regularization for the PITCR approach was found to be 0.10 for the case shown in Fig. 7 ($\alpha = 0.1$ and 17% undersampling).

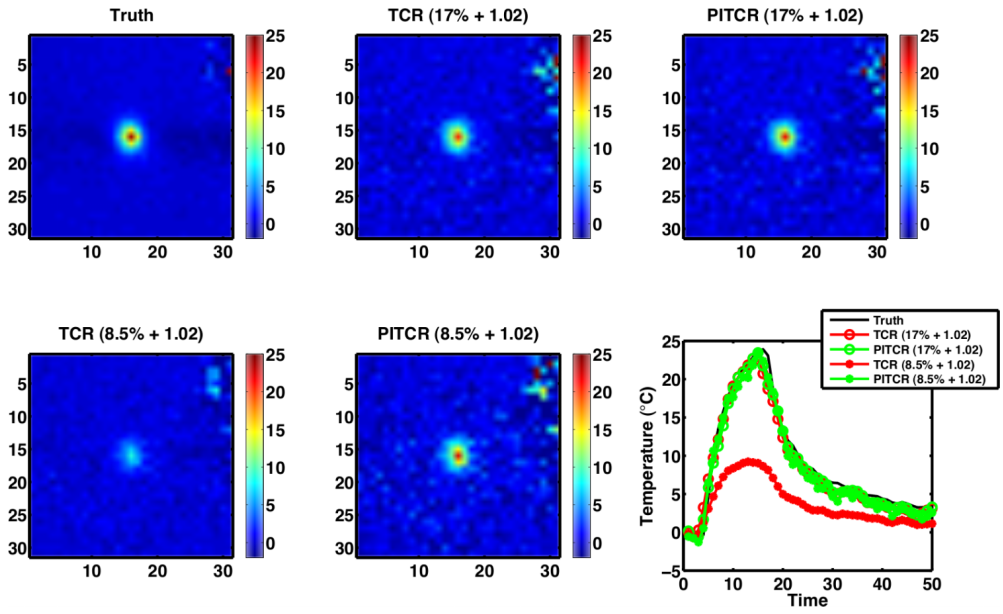

FIG. 4. Comparison of temperature map reconstruction of the standard TCR with PITCR method with noisy data. The percentage of sampling and noise (in °C) used is indicated in the parenthesis. The plots show the maximum temperature increase over time with 6× undersampling and for acquired 6× undersampled data further reduced by 50%.

in this case was found to be 0.0971 and 0.0911 for 17% and 8.5% data cases, respectively. The regularization parameter ($\tilde{\lambda}$) used for PITCR method was 0.005 for each of these cases.

To evaluate the proposed method with first frame based image reconstruction (similar to the one proposed using complex difference based compressive sensing[20]), the obtained undersampled MRI data (6× undersampling) and a further 50% reduction of this data was utilized. The reconstruction distribution pertaining to 17% and 8.5% measurements is shown in Fig. 5, along with the difference between the truth and the reconstructed temperature maps. This clearly indicates that the proposed method performs better than the first frame based reconstruction, as better prior information is included in the PITCR objective function. The regularization parameter used for PITCR and the first frame based method was 0.005. Another experiment was performed to verify the efficacy of the PITCR approach in the motion data case (motion generated outside the FOV by movement of the balloon). The obtained undersampled MRI motion data (6× undersampling) were used to reconstruct the image. The result pertaining to

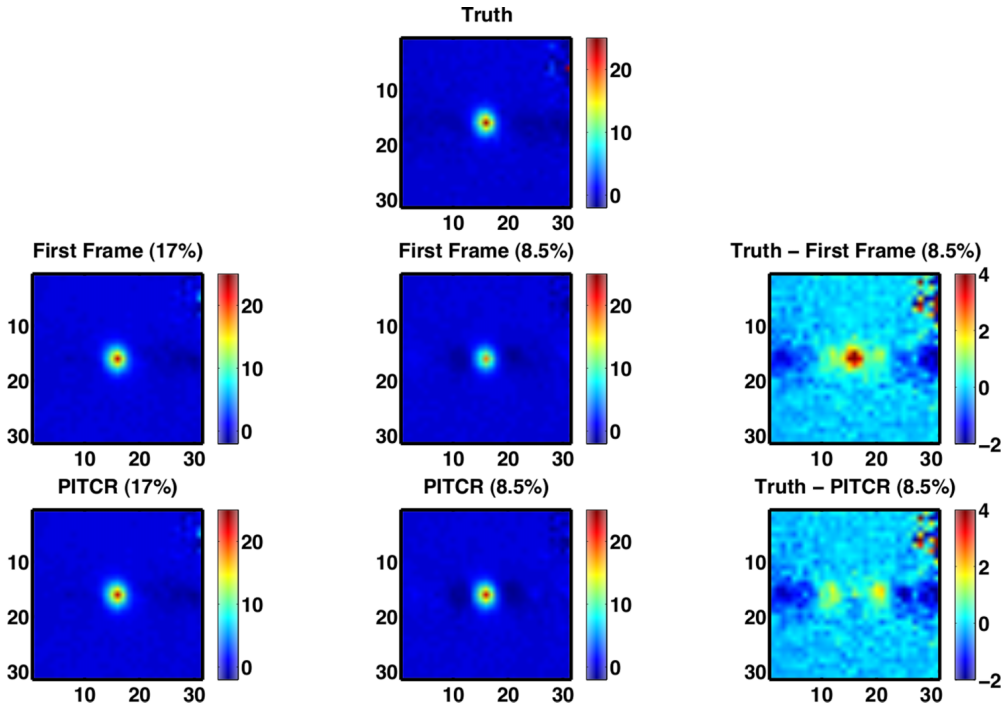

FIG. 5. Comparison of temperature map reconstruction of the first frame based image reconstruction with PITCR method. Difference image is also shown for better comparison of reconstructed temperature distribution. The percentage of sampling used is indicated in the parenthesis.

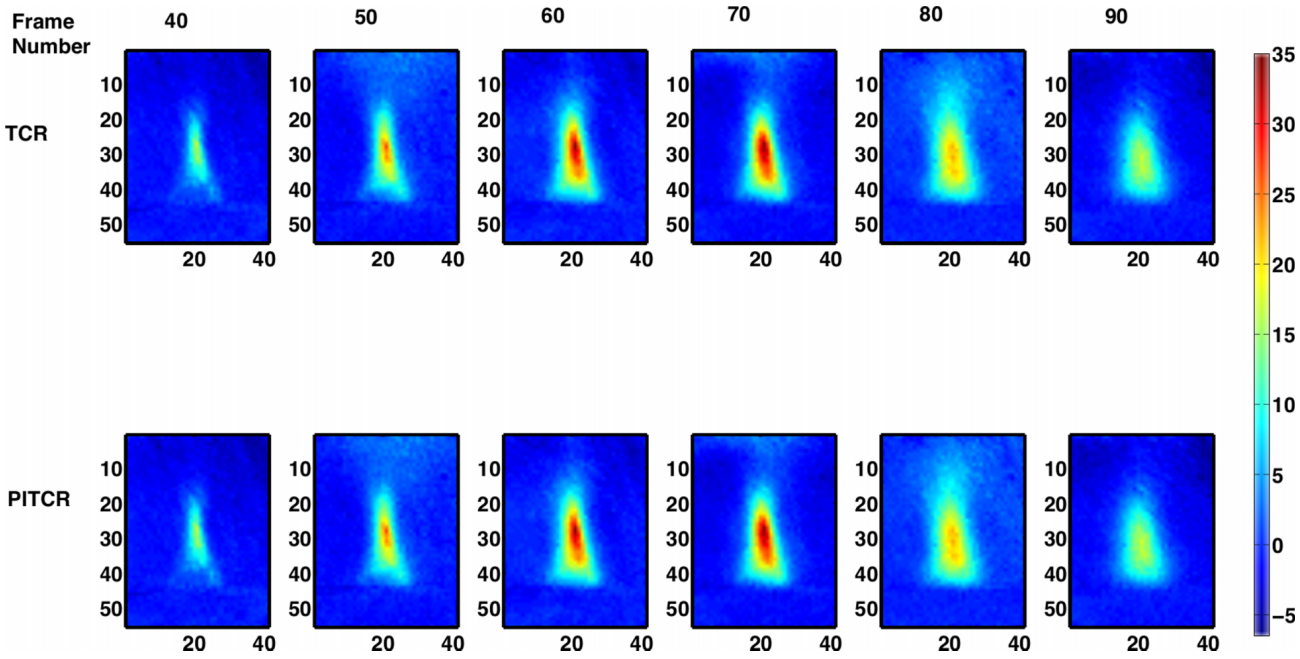

FIG. 6. Comparison of temperature map reconstruction of the standard TCR with PITCR method for motion data (outside the field of view) cases (6× undersampling data). The reconstructed temperature distribution along different frames is shown (it can seen that temperature is varying a lot due to motion). The difference between the TCR and PITCR methods is less than 1%.

the motion data case is shown in Fig. 6. Based on Figs. 1, 2 and 4–6, it can be concluded that the proposed scheme can be used in various settings like undersampled data cases, noisy environments, and motion outside the FOV. The regularization parameter for the TCR method was estimated as 0.071 using the L-curve approach, while 0.05 was used as the regularization parameter for the PITCR method.

Finally, the 6× undersampled dataset was used to study the effect of varying the weight factor (α) on the reconstruction results, which is indicated in Fig. 7. The optimal regularization parameter ($\tilde{\lambda}$) for each of the weights was obtained using the L-curve method shown in Fig. 3. The L-curve method to estimate $\tilde{\lambda}$ in the PITCR method was used only for these cases (as obtaining optimal $\tilde{\lambda}$ was computationally very expensive). Figure 7 indicates that the PITCR algorithm performs well within a range of weight factor (α). The optimal regularization parameters were 0.14 and 0.13 for the case $\alpha = 0.3$ with 17% and 8.5% data, respectively, 0.10 and 0.12 for the case $\alpha = 0.7$

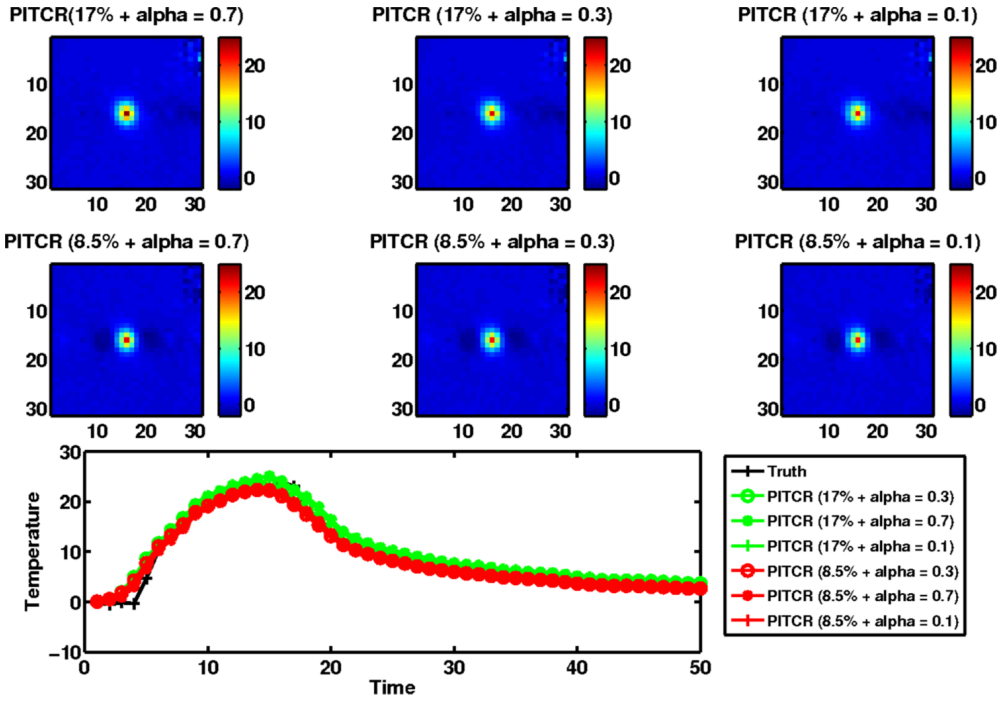

FIG. 7. Comparison of temperature map reconstruction of PITCR method for cases with different α values [Eq. (7)]. The plot shows the maximum temperature increase over time for the cases considered here.

with 17% and 8.5% data, and 0.0871 and 0.06 for the case with $\alpha = 0.1$ with 17% and 8.5% data.

4. DISCUSSION AND CONCLUSION

The performance of the PITCR method for the obtained MRgHIFU datasets was observed to be superior to the standard TCR approach (see Figs. 1, 2, 4, and 5) using highly undersampled data. The performance of the PITCR algorithm is similar to the TCR algorithm when the number of measurements available is high. Since the number of measurements required is less for the PITCR algorithm, this can result in faster data collection thereby reducing the scan time. The same data were used to obtain the temperature distribution for both TCR and PITCR algorithms. The PITCR method was also evaluated using noisy measurements (noise introduced by the coil) and even in the presence of noise the PITCR method was able to reconstruct the temperature maps more accurately than the TCR algorithm with fewer measurements.

Note that the proposed algorithm works better than the TCR algorithm as the prior constraint identifies the rise and fall in temperature more accurately than the TCR algorithm. The prior term in the objective function applies a higher order derivative constraint, enabling approximation of the maximum temperature rise/fall slope better than a simple temporal constraint. Recent works in x-ray CT have shown that usage of higher-order total variation along with a total-variation constraint results in a better solution than usage of a pure total-variation constraint.[25] Another work has used high-degree total variation and shown that it provides better image recovery compared to the total-variation approach.[26] The proposed approach uses a similar concept in a dynamic imaging framework (for MRgHIFU) to show that it requires fewer measurements to perform the temperature map reconstruction. The first frame based method in the constraint is not able to trace the slope (as shown in Fig. 5), because the constraint is imposed on the difference with the baseline alone rather than the increase or decrease in the temperature (which is obtained using prior images). The proposed scheme uses an ℓ_2-norm based constraint instead of ℓ_1-norm based as used in the original PICCS approach, because the change (rise or fall) in the temperature is gradual (relates to the smoothness). Hence, making use of isotropic total-variation would be more apt than anisotropic total-variation schemes. Utilization of sparsity transformation like wavelets and curvelets for converting the smooth rise in temperature as a sparse representation can be explored for performing PITCR in the ℓ_1-norm framework, but this is beyond the scope of the present study.

Table I indicates the time taken for reconstructing temperature maps using the TCR approach and the proposed PITCR method. The reported times indicate that the PITCR method is computationally expensive than the TCR algorithm. The reported reconstruction times does not include the time taken to estimate the optimal regularization parameter using the L-curve approach. The PITCR scheme was able to give a reasonable RMSE value (less than 1 °C at the ROI) when the data compression was very high (fewer measurements were acquired) as shown in Table I. Assuming the data-collection time is in the same scale as the reconstruction time, the PITCR algorithm can be used as an alternative to the TCR algorithm when fewer measurements are available, and the same can be inferred from Table I. At high acceleration factors like 6×, PITCR algorithm could be used to reconstruct the images retrospectively. In clinical use, it is important to obtain accurate temperature maps before the maximal temperature has reached to prevent overheating of tissue (damaging normal tissues). Note that even in these scenarios, the PITCR method is very efficient in obtaining accurate temperature maps, and this can be observed by the time-point by time-point comparison of the temperature rise (shown in Figs. 1, 2, and 4). Therefore, the performance of the PITCR method is better than the TCR method in cases of using a truncated dataset with only time points before the maximal temperature.

The proposed algorithm is computationally intensive as it requires estimation of an additional term in the gradient (three terms: prior term, temporal constraint, and data fidelity) as opposed to the TCR approach (two terms: temporal constraint and data-fidelity). Recent work had proposed a real-time TCR (RT-TCR) algorithm,[13] wherein the TCR algorithm was parallelized with graphics processing units (GPU's).[13] Thus, reconstructing the temperature maps faster than the data collection time in the dynamic sequence. As a part of future work, the PITCR algorithm would be rewritten for achieving massive parallelism using GPU.

There are two aspects to consider while comparing fully-sampled versus undersampled data sets designed to measure a dynamic process. The first aspect is related to the temporal resolution of the data. If the volume coverages are equal, the fully-sampled data will take longer to acquire, and the timing of the reconstructed image will be a complicated weighting of k-space data that were acquired at different points during the changing process of temperature rise/fall. On the other hand in the undersampled data case, the acquisition time is less and will be close to a "snap shot" of the process at the time of data acquisition. The second issue relates to the precision or temporal SNR. Fully sampled data have the advantage of more data points going into the reconstruction. However, data reconstructed with algorithms using constraints in the temporal dimension have the advantage of the constraint enforcing smoothness in time on the final 4D images. Reference 10 indicates that the temporal SNR of image data sets reconstructed from undersampled data using a temporal constraint can be higher than the fully-sampled data case.

The disadvantage of the PITCR algorithm is that it has two reconstruction parameters (α and $\tilde{\lambda}$) to be chosen compared to the TCR algorithm (which has only λ). The reconstruction parameter (λ) is selected optimally using a L-curve method in the TCR algorithm (as shown in Fig. 3), doing the same for multiple parameters in PITCR will be challenging. The reconstruction parameters were selected heuristically (to result in best possible temperature distribution) in the PITCR and first frame based method. The selection of regularization parameter ($\tilde{\lambda}$) in the PITCR approach can be done using the L-curve method, as indicated in Fig. 3. The optimal parameter selection for the PITCR method is computationally very expensive and

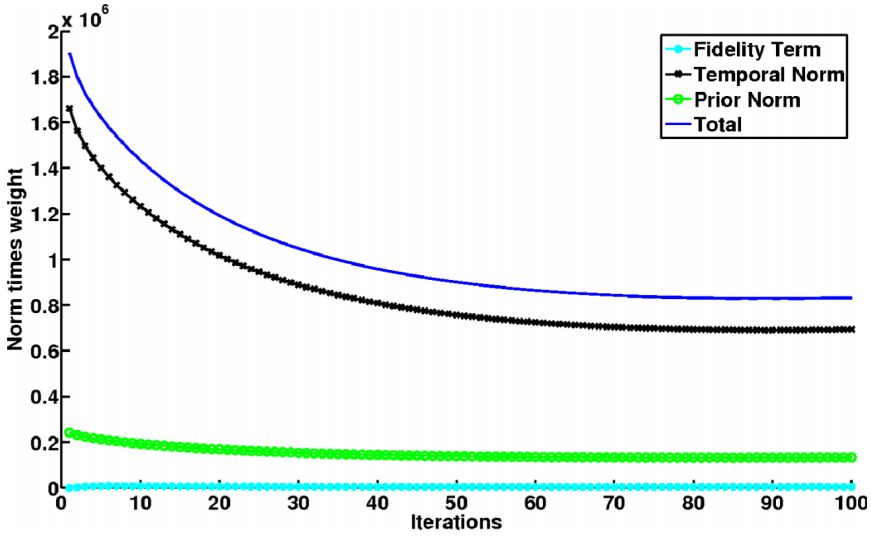

FIG. 8. The variation of the fidelity norm, prior term and the temporal gradient over gradient descent iteration in the PITCR approach for the case $\alpha = 0.3$ with 17% data shown in Fig. 7.

takes around five and half hours for the datasets used in this application. Therefore, the optimal regularization parameter was selected only in case of Fig. 7 (to study the effect of $\tilde{\lambda}$ and α variation) and for the rest of the cases this parameter was selected heuristically. Moreover, our observation has indicated that for a specific noise level, the regularization parameter does not vary much and can be fixed at a certain value. Reconstruction becomes more difficult as the number of reconstruction parameters to be estimated increases, thus the proposed algorithm was only compared with the TCR algorithm and not against model-based algorithms.

The sliding window k-space data are used as initialization in both the TCR and the PITCR algorithms. The data obtained from the sliding window lines (different phase encode lines compared to current time point data-acquisition) will be added to the undersampled data obtained at the current time frame, thereby obtaining the full k-space data for reconstruction. Moreover, the PITCR algorithm requires the next time frame (future time frame) for performing the image reconstruction. This additional constraint will create a delay in obtaining the reconstructed images by one acquisition cycle, which could be acceptable in many scenarios especially in cases requiring faster data acquisition. Figure 6 indicates that the PITCR algorithm is able to provide accurate reconstruction results in the presence of motion outside the region of interest, similar to the TCR approach. Hence, making the PITCR algorithm widely useful in scenarios where relatively fewer measurements are available to cases in which data are corrupted by motion and noise. Figure 8 indicates the convergence behavior of the PITCR method, and it can be clearly seen from the figure that the norm does not vary much using the PITCR approach even after 100 iterations.

In conclusion, a PITCR approach is proposed, which effectively uses the prior image for accurately providing the temperature map distribution with fewer measurements when compared to the existing TCR approach. The proposed scheme was found to be robust with noise when compared to the existing TCR approach with requiring relatively fewer measurements.

ACKNOWLEDGMENTS

The authors would like to acknowledge Dr. Stephen Starck and Sparchenzentrum, Technical University Munich for proofreading the paper. This work is supported by the Department of Biotechnology (DBT) Innovative Young Biotechnologist Award (IYBA) (Grant No. BT/07/IYBA/2013-13). J.P.'s work was supported by Microsoft Corporation and Microsoft Research India under the Microsoft Research India Ph.D. Fellowship Award and SPIE Optics and Photonics Education Scholarship.

APPENDIX: CONVERGENCE OF THE PITCR ALGORITHM

Even though the minimization used by the PITCR approach is performed using a gradient descent approach, deriving convergence for these set of algorithms tend to be difficult as the prior term is dynamically changing. Hence in this appendix, it is shown that if the proposed PITCR approach has at least one fixed point, then it converges to that fixed point. Note that the investigation about the existence of that fixed point is not studied here, as it is already present in Ref. 27. The current derivation of showing the solution converging to a existing fixed point is similar to the one presented in Ref. 28. Nonexpansive mapping theory is used in investigation about the fixed point. Nonexpansive mapping can have different characteristics like a mapping (K) is said to be strongly nonexpansive if K is nonexpansive and the sequences $(x_n)_{n\in\mathbb{R}}$ and $(y_n)_{n\in\mathbb{R}}$ are in $\mathbb{R}^{MNLT}$ such that $(x_n - y_n)_{n\in\mathbb{R}}$ is bounded and $\|x_n - y_n\|_2 - \|Kx_n - Ky_n\|_2 \to 0$ holds. Then the following $(x_n - y_n) - (Kx_n - Ky_n) \to 0$ also holds.[28,29] On the other hand, when K is firmly nonexpansive if $\forall x, y \in \mathbb{R}^{MNLT}$, $\|Kx - Ky\|_2^2 \le \langle (Kx - Ky),(x - y)\rangle$, where the definition of $\langle (Kx - Ky),(x - y)\rangle = \sum_{i=1}^{MNLT}((Kx)_i - (Ky)_i)(x_i - y_i)$.[28–30]

The operators used for the PITCR algorithms are nonexpansive. The gradient descent with enough iterations is strongly nonexpansive[27,31] and the temporal derivatives are proximal

mappings and hence are firmly nonexpansive.[32] All the operators used here are strongly nonexpansive and hence if K has at least one fixed point, then PITCR algorithm converges to that fixed point.[29,30]

[a]Electronic mail: pnjayaprakash88@gmail.com; +49893187-4727.

[1]P. P. Lele, "Production of deep focal lesions by focused ultrasound-current status," Ultrasonics **5**, 105–112 (1967).
[2]K. Hynynen, N. McDannold, G. Clement, F. A. Jolesz, E. Zadicario, R. Killiany, T. Moore, and D. Rosen, "Pre-clinical testing of a phased array ultrasound system for MRI-guided noninvasive surgery of the brain—A primate study," Eur. J. Radiol. **59**, 149–156 (2006).
[3]K. Hynynen, C. Damianou, A. Darkazanli, E. Unger, and J. F. Schenck, "The feasibility of using MRI to monitor and guide noninvasive ultrasound surgery," Ultrasound Med. Biol. **19**, 91–92 (1993).
[4]J. Hindman, "Proton resonance shift of water in the gas and liquid states," J. Chem. Phys. **44**, 4582–4592 (1966).
[5]B. Denis de Senneville, B. Quesson, and C. T. W. Moonen, "Magnetic resonance temperature imaging," Int. J. Hyperthermia **21**, 515–531 (2005).
[6]Y. Huang, J. Song, and K. Hynynen, "MRI monitoring of skull-base heating in transcranial focused ultrasound ablation," *Proceedings of ISMRM* (ISMRM, 2010), p. 249.
[7]C. Mougenot, M. O. Kohler, J. Enholm, B. Quesson, and C. Moonen, "Quantification of near-field heating during volumetric MR-HIFU ablation," Med. Phys. **38**, 272–282 (2011).
[8]J. Prakash, N. Todd, and P. K. Yalavarthy, "Advances in image reconstruction methods for real-time magnetic resonance thermometry," J. Indian Inst. Sci. **94**, 387–406 (2014).
[9]N. Todd, A. Payne, and D. L. Parker, "Model predictive filtering for improved temporal resolution in MRI temperature imaging," Magn. Reson. Med. **63**, 1269–1279 (2010).
[10]G. Adluru, S. P. Awate, T. Tasdizen, R. T. Whitaker, and E. V. Dibella, "Temporally constrained reconstruction of dynamic cardiac perfusion MRI," Magn. Reson. Med. **57**, 1027–1036 (2007).
[11]C. S. Mei, L. P. Panych, J. Yuan, N. J. McDannold, L. H. Treat, Y. Jing, and B. Madore, "Combining two-dimensional spatially selective RF excitation, parallel imaging, and UNFOLD for accelerated MR thermometry imaging," Magn. Reson. Med. **66**, 112–122 (2011).
[12]N. Todd, U. Vyas, J. de Bever, A. Payne, and D. L. Parker, "Reconstruction of fully three-dimensional high spatial and temporal resolution MR temperature maps for retrospective applications," Magn. Reson. Med. **67**, 724–730 (2012).
[13]N. Todd, J. Prakash, H. Odéen, J. de Bever, A. Payne, P. K. Yalavarthy, and D. L. Parker, "Towards real-time availability of 3-D temperature maps created with temporally constrained reconstruction," Magn. Reson. Med. **71**, 1394–1404 (2014).
[14]N. Todd, G. Adluru, E. V. R. Dibella, and D. Parker, "Temporally constrained reconstruction applied to MRI temperature data," Magn. Reson. Med. **62**, 406–419 (2009).
[15]G. H. Chen, J. Tang, and S. Leng, "Prior image constrained compressed sensing (PICCS): A method to accurately reconstruct dynamic CT images from highly undersampled projection data sets," Med. Phys. **35**, 660–663 (2008).
[16]G. H. Chen, J. Tang, and J. Hsieh, "Temporal resolution improvement using PICCS in MDCT cardiac imaging," Med. Phys. **36**, 2130–2135 (2009).
[17]W. A. Grissom, V. Rieke, A. B. Holbrook, Y. Medan, M. Lustig, J. Santos, M. V. McConnell, and K. B. Pauly, "Hybrid referenceless and multibaseline subtraction MR thermometry for monitoring thermal therapies in moving organs," Med. Phys. **37**, 5014–5026 (2010).
[18]P. Gaur and W. A. Grisson, "Direct reconstruction of proton resonance frequency-shift temperature maps from k-space data for highly-accelerated thermometry," *Proceedings of ISMRM, 2013*.
[19]P. Gaur and W. A. Grisson, "Accelerated MRI thermometry by direct estimation of temperature from undersampled k-space data," Magn. Reson. Med. **73**, 1914–1925 (2015).
[20]Z. Cao, S. Oh, R. Otazo, C. T. Sica, M. A. Griswold, and C. M. Collins, "Complex difference constrained compressed sensing reconstruction for accelerated PRF thermometry with application to MRI-induced RF heating," Magn. Reson. Med. **73**, 1420–1431 (2015).
[21]M. Lustig, D. Donoho, and J. M. Pauly, "Sparse MRI: The application of compressed sensing for rapid MR imaging," Magn. Reson. Med. **58**, 1182–1195 (2007).
[22]P. C. Hansen and D. P. O'Leary, "The use of the L-curve in the regularization of discrete ill-posed problems," SIAM J. Sci. Comput. **14**, 1487–1503 (1993).
[23]J. N. Tehrani, A. McEwan, C. Jin, and A. V. Schaik, "L1 regularization method in electrical impedance tomography by using the L1-curve (Pareto frontier curve)," Appl. Math. Modell. **36**, 1095–1105 (2012).
[24]H. Odeen, N. Todd, M. Diakite, E. Minalga, A. Payne, and D. L. Parker, "Sampling strategies for subsampled segmented EPI PRF thermometry in MR guided high intensity focused ultrasound," Med. Phys. **41**, 092301 (14pp.) (2014).
[25]Y. Zhang, W. H. Zhang, H. Chen, M. L. Yang, T. Y. Li, and J. L. Zhou, "Few-view image reconstruction combining total variation and a high-order norm," Int. J. Imaging Syst. Technol. **23**, 249–255 (2013).
[26]Y. Hu and M. Jacob, "Higher degree total variation (HDTV) regularization for image recovery," IEEE Trans. Image Process. **21**, 2559–2571 (2012).
[27]C. H. Morales and C. E. Chidume, "Convergence of the steepest descent method for accretive operators," Proc. Am. Math. Soc. **127**, 3677–3683 (1999).
[28]C. Mory, V. Auvray, B. Zhang, M. Grass, D. Schafer, S. J. Chen, J. D. Carroll, S. Rit, F. Peyrin, P. Douek, and L. Boussel, "Cardiac C-arm computed tomography using a 3D + time ROI reconstruction method with spatial and temporal regularization," Med. Phys. **41**, 021903 (12pp.) (2014).
[29]H. H. Bauschke, V. Martin-Marquez, S. M. Moffat, and X. Wang, "Compositions and convex combinations of asymptotically regular firmly nonexpansive mappings are also asymptotically regular," Fixed Point Theory Appl. **2012**(1), 53 (11pp.).
[30]H. H. Bauschke and P. L. Combettes, "The Baillon-Haddad theorem revisited," preprint arXiv:0906.0807 (2009).
[31]Z. Xu and G. F. Roach, "A necessary and sufficient condition for convergence of steepest descent approximation to accretive operator equations," J. Math. Anal. Appl. **167**, 340–354 (1992).
[32]N. Parikh and S. Boyd, "Proximal algorithms," Found. Trends Optim. **1**, 127–239 (2013).